Failure of polyamide 11 using a damage finite elements model

Guillaume Boisot, C. Fond, Gilles Hochstetter, Lucien Laiarinandrasana

Failure of PolyAmide 11 using a Damage Finite Elements Model

G. Boisot[1, 2, 3, a], C. Fond[1, b], G. Hochstetter[2, c] and L. Laiariandrasana[3,d]

[1]Institut Charles Sadron / CNRS – UPR 22 / 23 rue du Loess / 67034 Strasbourg Cedex 2/ BP 84047 / France

[2]ARKEMA Cerdato / Route du Rilsan / 27470 Serquigny, France

[3]MINES ParisTech, Centre des Matériaux, CNRS UMR 7633, BP 87 91003 Evry Cedex, France

[a]guillaume.boisot@ensmp.fr, [b]cfond@ics.u-strasbg.fr, [c]gilles.hochstetter@arkemagroupe.com, [d]lucien.laiarinandrasana@ensmp.fr

Keywords: polymer, mechanics, fracture, damage, polyamide 11.

Abstract. The present paper focuses on the mechanical properties and the damage of the polyamide 11 at 0°C. Thanks to experimental investigations on smooth specimen and Circumferentially Notched Round Bar (CNBR) combined with observations by Scanning Electon Microscopy (SEM), the Gurson-Tvergaard-Needleman model [1] has been set up to give an account of the viscoplastic behavior and the damage of the PA11. The case study is concerned damage mechanics and fracture mechanics. The co-existence of two formulations of the material failure can then be cited: a volume approach or a surface one (cohesive zone [2], XFEM [3]). This paper focuses only on the damage mechanics and its modeling. Therefore the failure criterion is a critical porosity criterion.

Introduction

Produced from a renewable source (castor oil), the polyamide 11 (PA11 or also known as Rilsan®) is a semi-crystalline polymer used in a large number of applications thanks to its properties: excellent resistance to chemicals, ease of processing, a wide range of working temperature (-40°C/ +130°C), a low density, to name a few. Rilsan® can be found in many industries therefore. The one which has been investigated in this work is used in pipe form for the natural gas distribution. For rapid and economical installation it is difficult to beat coiled plastic pipe. For higher pressure it is now possible to install coiled polyamide 11 (PA11) gas pipe instead of steel. Coiled pipe offers cost advantage in the form of reduced installation costs as well as the elimination of a cathodic protection system. To go further in the use of polyamide 11 such as toughened polyamide 11 for instance and thus to create a more relevant material for specific uses, it is necessary to study the mechanical behavior as well as the damage development of this material. In this paper both are investigated at 0°C over a wide range of loading conditions. Experimental tests were carried out at various strain rates on smooth, notched and cracked specimens. Finite elements simulations are fulfilled using the Gurson model [1] firstly adapted to the present material.

Material and Experimental Procedures

The material.

The material of the study is provided by ARKEMA; it has been extruded without plasticizer and has not been aged. An initial amount of porosity has been evidenced and evaluated thanks to microscopic observation of a sample broken in liquid nitrogen. The initial porosity was found equal to 1%. The PA11 whitens when loaded; whitening is related to cavitation occurring within the material by voids growth which generates a volume change. Moreover, for this kind of polymeric material, the complete failure is assumed to be probably preceded by the nucleation, growth, fibrillation and coalescence of voids. Some key properties are summarized in the Tab 1. DSC

(Differential Scanning Calorimetry) as well as DMA (Dynamic Mechanical Analysis) have been performed. The Fig. 1 shows the evolution of the Young modulus (MPa) and the Poisson ratio (-) in function of the temperature (°C).

Melting point	184-188 °C
Index of crystallinity	20-25 %
Glass transition	40 °C
Young modulus	1500 MPa
Poisson ratio	0.42

Tab 1: Key properties of the investigated material

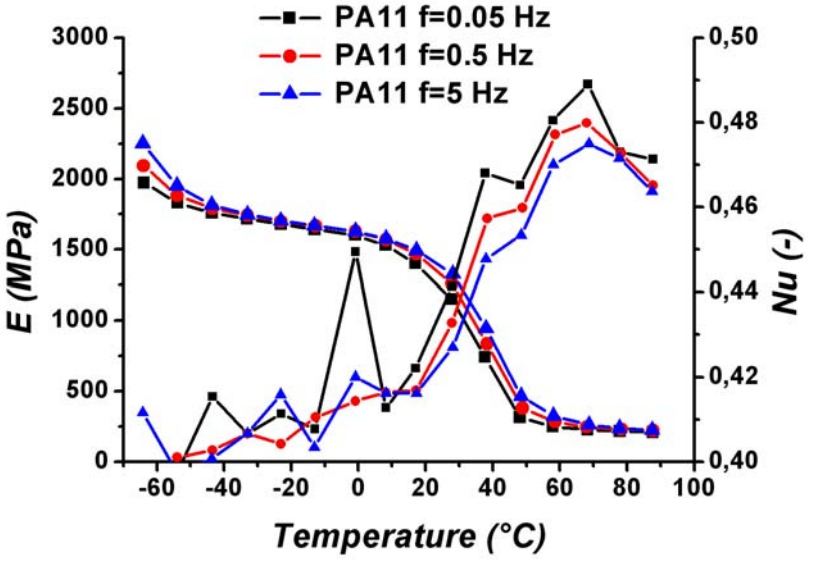

Fig. 1: Young Modulus (MPa) and Poisson ratio (-) evolution in function of the temperature

Experimental procedure.

Tensile tests have been performed on two main kinds of geometry: smooth and Circumferentially Notched Round Bar (CNRB) specimens. Smooth specimens were manufactured from 6mm extruded sheets with a gauge length of 100 mm and a cross section of 10*4 mm². An Inströn testing machine is used to carry out the tests at several strain rates (1 s^{-1}, 0.1 s^{-1}, 0.01 s^{-1}, and 0.001 s^{-1}) at a temperature of 0°C. A strain gage extensometer with a gauge length of 25 mm is also used.

Regarding the CNRB tensile tests, four notch radii were involved: 4, 1.6, 1.2 and 0.8 mm. The nomenclature used in the document for these geometries is the following one: for a given notch radius *R*, the relative geometry is written CNRB R; for instance CNRB 1.6 for a notch radius of 1.6 mm. CNRB specimens have a length of 85 mm; the diameter of the minimal section is equal to 4 mm and the maximum diameter is 7.2 mm. A strain gage is positioned at the notch tip in order to record the diametrical reduction of the minimal section. Tests are carried out by controlling the crosshead displacement (0.05 $mm.s^{-1}$) which is also measured. Both tensile tests (on smooth and CNRB specimens) are performed at a temperature of 0°C.

Results of the Experimental Investigation

Tensile tests on smooth specimens.

Nominal stress-strain curves on smooth specimens are shown in Fig. 2 for the four strain rates. It emphasizes the strong influence of the strain rate. The maximum load increases by roughly 30% from 0.001 s-1 to 1 s-1 regarding the strain rate. Increasing the strain rate tends also to reduce the nominal strain at failure.

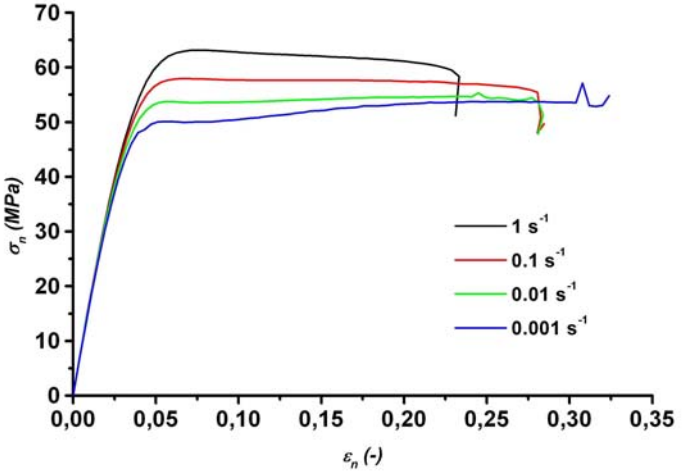

Fig. 2: Nominal stress (MPa) vs nominal Strain (-) on smooth specimen for various strain rates at 0°C

Tensile tests on CNRB specimens.

The results for the CNRB tensile tests are shown Fig. 3. More exactly it deals with the nominal stress (MPa) vs the adimensional ratio based on the diametrical reduction (-), respectively defined as follows:

$$\sigma_n = \frac{F}{\pi . a_0^2} . \tag{1}$$

$$\log(\frac{a_0^2}{a^2}) . \tag{2}$$

With the load F and a_0 the initial radius of the minimal section (equal to 2 mm for these samples). The adimensional ratio would be equivalent to the local mean longitudinal strain in the case of a constant volume. In the opposite case (non constant volume which occurs in this model) this variable underestimates it. Notched specimens are really interesting to work with as they combine a quite comprehensive geometry also easy to machine and a huge range of stress state at the notch tip thanks to the variable notch radius. Indeed it has been proved that decreasing the notch radius which corresponds to increasing the stress triaxiality ratio (τ) results in an increase of the maximum load [4, 5]. The plateau observed after the post-yield softening is the result of the

competition between the softening caused by the void growth and the hardening due to the chain elongation.

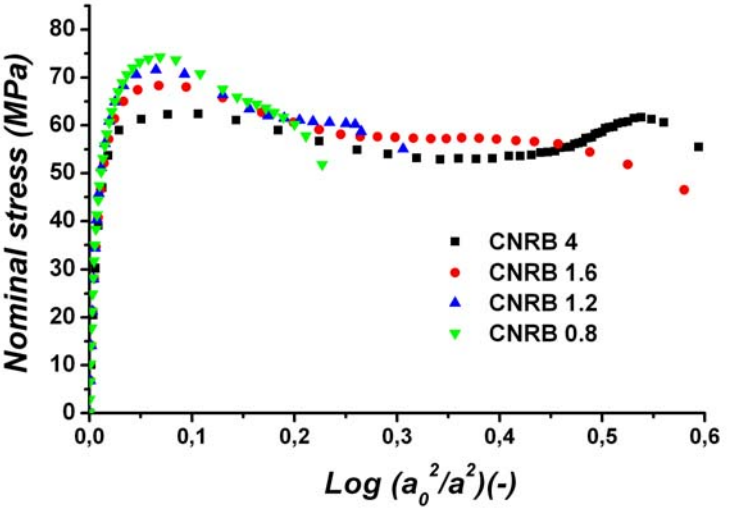

Fig. 3: Experimental curves for 4 notch radii

Microscopic observations

Experimental procedure.

Interrupted tensile tests on the CNRB specimens have been carried out to highlight the damage development as well as the deformation localization. Only three radii have been investigated: 4, 1.6 and 0.8 mm. Thanks to the strain gage positioned at the notch tip, the test is interrupted when the diametrical reduction reaches 40%. The sample is cut a first time to keep only the notched part and then after having spent a time in liquid nitrogen cut a second time to minimize the use of the microtome in order to reach the core of the specimen. The sample is then microtomed along the tensile direction. Then SEM observations of the longitudinal cross sections are performed enabling to create a porosity mapping along the minimal cross section. The amount of voids is determined by digital image processing, its definition being the area fraction of cavities.

Influence of the stress triaxiality ratio on the damage.

Whatever the investigated notch radius, void growth is localized in the minimal cross section mainly in the core of the specimen and do not extend further in the longitudinal direction (Fig. 4). Fig. 5 exhibits the amount of the porosity along the minimal cross section for the 3 investigated notch radii and emphasizes the influence of the stress triaxiality ratio on the damage. Namely the increase of the stress triaxiality ratio (equivalent to the decrease of the notch radius) leads to a raise of the amount of the porosity; the higher the stress triaxiality ratio, the more extended along the minimal cross section the porosity.

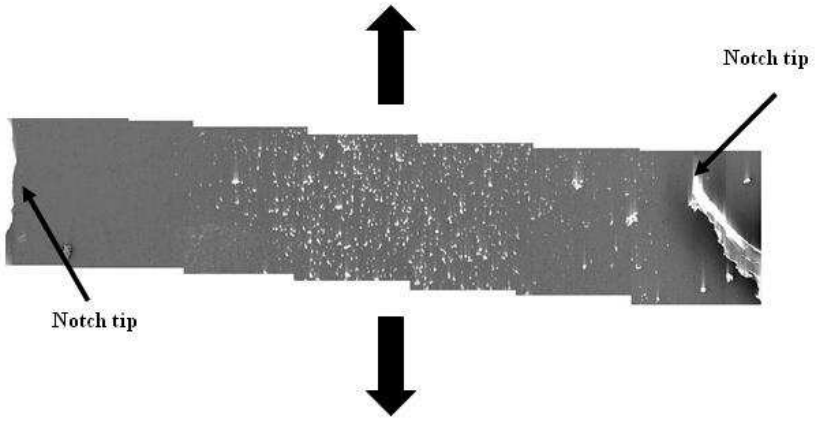

Fig. 4: Porosity mapping along the minimal cross section (CNRB 4; *200)

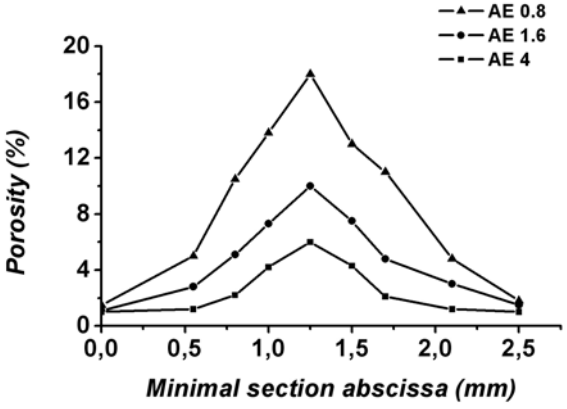

Fig. 5: Porosity along the minimal cross section for 3 notch radii

Modelling

The modified GTN model.

The used model to simulate the mechanical behavior and the damage of the polyamide 11, is based on the Gurson's yield function [1] extended by Tvergaard and Needleman [6, 7]:

$$\Phi(\sigma,\sigma_y,f) = \frac{\sigma_{eq}^2}{\sigma_y^2} + 2q_1.f.\cosh\left(\frac{q_2\sigma_{kk}}{2\sigma_y}\right) - (1+f^2) = 0. \quad (2)$$

Where σ_{eq} is the von Mises Stress, σ_{kk} the trace of the stress tensor and f is the porosity. q_1 and q_2 are two parameters introduced to improve the model predictions for periodic arrays of cylindrical and spherical voids [4]. The yield surface is expressed as:

$$\Phi = \sigma^* - R. \quad (3)$$

R is the flow stress of the matrix. The viscoplastic strain rates tensor is given by the normality rule as:

$$\underline{\dot{\varepsilon}} = (1-f)\dot{p}\frac{\partial \Phi}{\partial \underline{\sigma}}. \tag{4}$$

so that

$$(1-f)\dot{p}\sigma^{*} = \underline{\sigma} : \underline{\dot{\varepsilon}}_{p}. \tag{5}$$

To express the matrix viscoplatic law, a Norton law will be used, defined as follows:

$$\dot{p} = \left(\frac{\Phi}{K}\right)^{n}. \tag{6}$$

The evolution of porosity is expressed using mass conservation:

$$\dot{f} = (1-f)trace(\underline{\dot{\varepsilon}}). \tag{7}$$

The material flow stress is expressed as:

$$R = R_0 + Q(1-\exp(-bp) + A(\exp(Bp)-1) \tag{8}$$

$Q(1-\exp(-bp)$ describes the initial hardening stage supposed to be isotropic whereas $A(\exp(Bp)-1)$ allows to simulate the large stretching of the fibrils [4]. The parameters q_1 and q_2 have been introduced to take the damage evolution into account: q_1 is expressed as the inverse of the critical porosity (f_c); q_2 is expressed as a function of the maximum principal plastic strain p_1. Initially the cavities are assumed spherical but they tend to become oriented and elongated during the test that is why to describe this phenomenon, q_2 is a function of p_1 as follow:

$$q_2 = (M-m)\times\frac{(\tanh(v(p_t - p_1))+1)}{2} + m. \tag{9}$$

Model identification.

Several parameters need to be identified. The first ones which are R_0, K, n, are determined thanks to the experimental investigations on the smooth specimens by using the nominal stress-nominal strain curves at various strain rates. The Fig. 5 shows the curves obtained by FE simulations compared with the experimental ones.

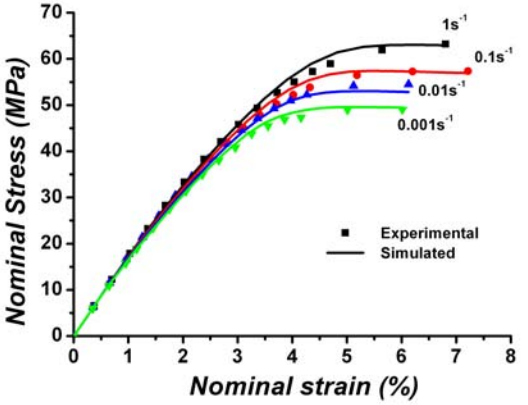

Fig. 6: Comparison between the simulated and experimental curves in the case of the smooth specimens

Tensile tests on the smooth specimens give approximate values of the parameters R_0, Q and b. The modelling of the tensile tests of the CNRB specimens enables to define them more accurately. Moreover the strain-hardening parameters (A and B) can only be identified using the CNRB experimental results. The Fig. 6 shows the results of the simulations on the CNRB. To handle the evolution of porosity, the parameters q_1 and q_2 need to be set: their settings are achieved thanks to the SEM observations mainly which emphasize the range of values for both parameters and also with simulations on Single Edge Notch Bar (SENB) testing in 3 points bending. It has been shown for the PVDF that at low stress triaxiality rate, failure occurs when the plastic strain reaches a critical value p_c and for higher stress triaxiality ratio, failure occurs when the void growth reaches a critical value f_c [8]. Thus damage parameters could be more accurately defined.

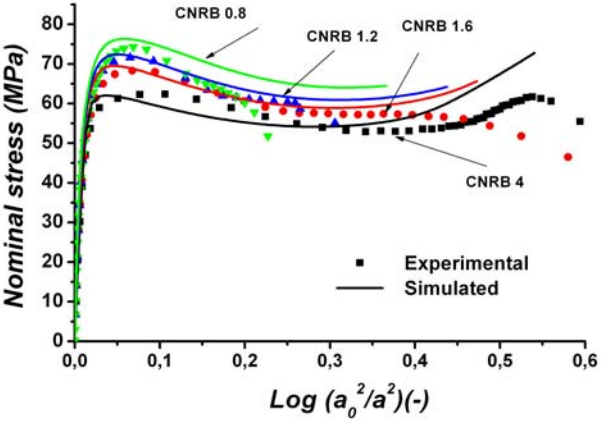

Fig. 7: Comparison between the simulated and experimental curves in the case of the CNRB specimens

Results.

The model accounts for the mechanical behavior of the material characterized by the damage by void growth loading to a softening and the strain-hardening by chains elongation. Furthermore the parameter q_2 enables to initiate the failure either at the notch tip or at the core.

Conclusion and Future Works

The viscoplastic behavior and the damage of the polyamide 11 have been investigated in this paper. Experimental investigations on smooth and CNRB specimens combined with SEM observations of interrupted tests highlights that damage is mainly caused by void growth. To model the mechanical behavior of the PA11 and thus the softening by void growth as well as the strain-hardening due to the chains elongation, a constitutive model is used. To go further in these investigations, it may be interesting to run some more experimental tests on CNRB with a lower notch radius in order to increase the stress triaxiality ratio. Observations of fracture surfaces added to FE simulations may be relevant to define the parameters q_1 and q_2 more accurately and to better understand the competition between damage and fracture mechanics.

References

[1] A.L. Gurson: Continuun Theory of Ductile Rupture by Void Nucleation and Growth: Part 1- Yield Criteria and Flow Rules for Porous Ductile Media. J. Eng. Mater. Technol. Vol. 99 (1977), p. 2-15

[2] R. Estevez, , M. G. A. Tijssens, E. van der Giessen: Modeling of the Competition Between Shear Yielding and Crazing in Glassy Polymers. Journal of the Mechanics and Physics of Solids, 48 (2000) 2585–2617

[3] J.F. Unger, S. Eckardt, C. Könke: Modelling of Cohesive Crack Growth in Concrete Structures with the Extended Finite Element Method. Comput. Methods Appl. Mech. Engrg., Vol. 196 (2007), 4087-4100

[4] M. Challier, J. Besson, L. Laiarinandrasana, R. Piques and S. Pignoc: Damage and Fracture of PVDF at 20°C: Experiments and Modeling. Eng. Frac. Mech. Vol. 73 (2006), p. 79-90

[5] P.W. Bridgman: Trans Am Soc Met (1944), 32, 553

[6] V. Tvergaard: Influence of Voids Nucleation on Ductile Shear Fracture at a Free Surface. J. Mech. Phys. Solids Vol. 30 (1982), 399-425

[7] V. Tvergaard and A. Needleman: Analysis of the Cup-Cone Fracture in a Round Tensile Bar. Acta Metall. Vol. 32 (1984), 157-169

[8] M. Lafarge: Modélisation Couplée Comportement Endommagement et Critères de Rupture dans le Domaine de la Transition du PVDF. Thesis, Mines Paris, France, 2004.